Supplementary Information:
Interplay of lithium intercalation and plating in single graphite particle

Tao Gao,[1] Yu Han,[1] Dimitrios Fraggedakis,[1] Supratim Das,[1] Tingtao Zhou,[2] Che-Ning Yeh,[3] Shengming Xu,[4] William C. Chueh,[3] Ju Li,[5,6] and Martin Z. Bazant[1,7,*]

[1] *Department of Chemical Engineering, Massachusetts Institute of Technology, MA 02139.*

[2] *Department of Physics, Massachusetts Institute of Technology, MA 02139.*

[3] *Department of Material Science and Engineering, Stanford University, CA 94305*

[4] *Institute of Nuclear and New Energy Technology, Tsinghua University, Beijing 100084, China.*

[5] *Department of Nuclear Science and Engineering, Massachusetts Institute of Technology, MA 02139.*

[6] *Department of Material Science and Engineering, Massachusetts Institute of Technology, MA 02139.*

[7] *Department of Mathematics, Massachusetts Institute of Technology, MA 02139.*

CHEMICAL POTENTIAL AND VOLTAGE

To better understand the experiment results, especially to relate the observed voltage-capacity curve with the intercalation and phase transition of graphite as well as Li plating (Fig.S7), we derive the equation to relate observed voltage with chemical potential using chemical kinetics based on non-equilibrium thermodynamics.[1]

In this experiment, the intercalation reaction happening at the working electrode (HOPG particle) and the redox reaction at the reference electrode (Li metal) can be written respectively as:

$$Li^+ + e^- + M \iff LiM \tag{S1}$$

$$Li^+ + e^- \iff Li \tag{S2}$$

At the working electrode, Li^+ intercalates into the host structure of graphite, consumes one electron, occupies one interstitial site from the host (M) and generates one Li-e polaron (LiM). At the reference electrode, Li^+ is reduced by one electron and deposits as Li atom.

The affinity A, which is the difference in chemical potential between the products and reactants, equals $e\eta$ and measures the driving force of the reaction. The affinity for each reaction S1 and S2 are

$$A_w \equiv e\eta_w = \mu_{LiM} - \mu_M - (\mu_{Li^+,w} + e\phi_{l,w} - e\phi_{s,w}) = \mu_s - (\mu_{Li^+,w} + e\phi_{l,w} - e\phi_{s,w}) \tag{S3}$$

$$A_r \equiv e\eta_r = \mu_{Li} - (\mu_{Li^+,r} + e\phi_{l,r} - e\phi_{s,r}) \tag{S4}$$

in which subscripts l, s, w, r refer to liquid phase (electrolyte), solid phase (electrode), working electrode and reference electrode, respectively. ϕ is electrostatic potential. μ is the chemical potential of each species in the reaction. μ_s is the diffusional chemical potential at the graphite edge surface, which measures the energy change when a vacancy in the host (M) is replaced by a polaron (LiM). η_w and η_r are the overpotential for the reactions at working and reference electrode.

The half cell potentials $\Delta\phi$, defined as $\phi_s - \phi_l$ for each electrode, are

$$\Delta\phi_w = -\frac{\mu_s}{e} + \frac{\mu_{Li^+,w}}{e} + \eta_w \tag{S5}$$

$$\Delta\phi_r = -\frac{\mu_{Li}}{e} + \frac{\mu_{Li^+,r}}{e} + \eta_r \tag{S6}$$

The measured voltage in the experiment is the difference in the electrostatic potential between the working and reference

$$V = \phi_w - \phi_r = \Delta\phi_w - \Delta\phi_r + (\phi_{l,w} - \phi_{l,r}) = -\frac{\mu_s - \mu_{Li}}{e} + \frac{\mu_{Li^+,w} - \mu_{Li^+,r}}{e} + (\eta_w - \eta_r) + (\phi_{l,w} - \phi_{l,r}) \tag{S7}$$

The equation can be greatly simplified at equilibrium. At equilibrium, there is no reaction so overpotential is zero. There is no gradient in the electrolyte electrostatic potential or chemical potential of Li^+ leading to $\mu_{Li^+,w} \simeq \mu_{Li^+,r}$ and $\phi_{l,w} \simeq \phi_{l,r}$. Using the chemical potential of Li metal as the reference for chemical potential, the measured voltage is

$$V = -\frac{\mu_s}{e} \tag{S8}$$

which suggests that the open circuit voltage of the battery directly reflects the diffusional chemical potential of graphite.

In a typical experiment, the applied current, 50 μA, corresponds to a current density of 1.25 mA/cm^2, which is much smaller than the diffusion limiting current $J_{lim} = 2c_0FD/(t_aL) \approx$ 84 mA/cm^2 for a particle thickness of 100 μm and separator thickness of 10 μm. Therefore, the gradient in the electrolyte electrostatic and chemical potential of Li^+ are negligible. In addition, the reaction on the reference electrode is facile so $\eta_r \approx 0$. We have

$$V \approx -\frac{\mu_s}{e} + \eta_w \tag{S9}$$

CHEMICAL POTENTIAL AND PHASE TRANSITION

The diffusional chemical potential as a function of local concentration is given in Fig. S8. The vertical dash line shows the binodal region. Once the local concentration enters the binodal region and crosses spinodal point, phase separation happens. During lithiation, the surface concentration of HOPG increases, and the blue-red phase transition is triggered once c_s is over 0.2, which means the c_s will jump to 0.5 once the red phase forms. After that, c_s will continue to increase, and the red-gold phase transition will be triggered once c_s enters the second spinodal region.

BLACK FLOC-LIKE MATTER FORMED DURING LI DISSOLUTION

We hypothesize this is micron-sized lithium covered by nanometer thick solid electrolyte interface (SEI). Bulky lithium metal shows a silver color. The color transforms to black, however,

when the particle size reduces into micron regime. This happens because the dissolution reaction is intrinsically a corrosion reaction. During the transition of bulky lithium to stacking of micron-particles of lithium, it loses both the shining color. Once all bulk lithium has been transformed into micron-particles, the percolating pathway for electrons is lost since the particles are separated by the surface film, which is highly ionic conductive but electronic insulating. Therefore, oxidation of these small particles becomes kinetically difficult (happening at plateau of 400 mV).

THE SOURCE OF LI FOR THE PLATED PHASE

The source of Li for the plated phase is still under debate. In pure metallic substrate, such as Cu [2], it is clear that the Li reservoir is the electrolyte itself. However, when plating occurs on an intercalation material, such as graphite, then a second 'source' of Li might be considered. In particular, we can think of the intercalated Li to be converted into plated Li. In order to understand if this is the case, we need to resort to a picture which involves the electrostatics at the graphite/Plated Li contact.

In general, it is well known that the metallic Li has lower work function than C_6 and LiC_6. This can be translated in terms of the Fermi level of each material, i.e. C_6 and LiC_6 have lower Fermi energy than Li metal [3]. Therefore, when we put in contact the two materials, electrons are going to flow from the material with high electronic energy to the low one (from Li metal to graphite). Because of the metallic nature of both Li metal and Li_xC_6, surface charges will build up on the two interfaces. More specifically, Li metal and C_6/LiC_6 will have positive and negative charges, respectively. Additionally, an electric field $\mathbf{E}$ will build up on the contact between the two different phases, which will point towards the graphite, Fig. S10. To first order approximation, one can consider the electrostatic force on the holes ('bare' Li ions) to be $\mathbf{F} = q\mathbf{E}$, so the surface Li ions would like to be detached from the plated Li and enter the graphite. Moreover, Li exists inside graphite as an ion [3], and thus there is an attractive force between the Li^+-e^- pairs inside graphite. According to this physical picture, it is highly unlikely for the intercalated Li to want to leave its host material, C_6. To this end, using these first order assumptions, we conclude that the major Li source for the plated Li is electrolyte.

MATHEMATICAL MODEL

The model system is a layered sandwich of a lithium reference electrode, electrolyte layer, plated lithium (after it starts growing) and active particle graphite, in that order from left to right. We define all potentials with respect to the equilibrium potential of Li/Li^+. The electrolyte layer in contact with the reference lithium electrode is considered to be an infinite reservoir of lithium ions. Current applied during the charging (lithiation of graphite) step is assumed positive as a convention. Kinetics for intercalation is described using a formulation for concerted transfer of ions and electrons in non-equilibrium conditions. Kinetics of the side reaction (lithium plating) is described using a Butler-Volmer formulation with a pre-factor that scales with the volume of lithium deposited per unit area. Lithiated graphite is known to spontaneously phase separate at certain concentrations in the free-energy landscape which gives rise to the 'staging' behavior. Multi-variable frameworks accounting for two/three layer interactions of ions can mostly describe lithium intercalation at high-filling fractions, but it cannot easily describe the plethora of stable or metastable phases in graphite at low-filling fractions (not only for lithium), which exhibit longer range periodicity across three or more layers. To capture this staging, we use a single-variable free-energy model for lithium intercalation in graphite, developed by Alyea et al. [4]. The expression is fitted to the open circuit voltage at low filling fractions as an effective solid solution, while still captures the two primary voltage plateaus at high filling fractions. The free energy permits construction of two common tangents between filling fractions near 0.3 and 0.5 and another between filling fractions near 0.5 and 0.9 which leads to the two clear voltage plateaus and two sharp moving fronts.

Validation: Validation of a 1D model using experimental data on a mm scale graphite particle involves a few steps to simplify the experimental system being studied. We assume isotropic solid diffusivity, and extract a small vertical slice (around 50x500 pixels in dimension) from the top left of the particle (shown in Red dotted lines in Figure 2b on Particle A in main text). The jagged edge slope of the HOPG particle is removed digitally to prevent erroneous readings from image processing. The final snipped image is contrast-enhanced and then processed using an algorithm, assisted by the MATLAB Image Processing Toolbox, to convert the observed colors on graphite to a time-dependent solid-phase concentration map. The image processing does not change the signature of the colors in any way. This concentration profile used to compare theoretical predictions of the time evolution of plated lithium volume from the model. Parameters in the theory are obtained from fitting to the lithiation voltage curve from multiple repeats of the experiment.

Thermodynamics: The expression for μ_h is taken from Appendix A of Ref [4]. The non-homogeneous chemical potential can be obtained by taking the derivative of the gradient energy penalty term, following Cahn and Hilliard [5], $\mu_{nh} = -\kappa\nabla^2 c$. Combining these two expressions we get,

$$\mu = \frac{\delta G}{\delta c} = \mu_h - \kappa\nabla^2 c \tag{S10}$$

Diffusivity: Persson et al. [6] studied the energetics of stage I and stage II graphite intercalation compounds using a generalized gradient approximation (GGA) to density functional theory (DFT), and employed Kinetic Monte-Carlo simulations to calculate lithium diffusion coefficients as a function of lithium concentration. Since stages I and II dominate the lithium-graphite phase diagram, we directly use the results given in log-linear plot in Figure 3 in Ref. [6] to describe D as a function of $\tilde{c}$ (scaled to the electrolyte concentration c_{max}) using a straight line. The best fit linear relations obtained from the data are:

$$log_{10}\left(D\ [cm^2/s]\right) = \begin{cases} -5.55\ \tilde{c} - 6.69 \ \text{ if } \tilde{c} \leq 0.5\ (stage\ II) \\ -2.21\ \tilde{c} - 7.15 \ \text{ if } \tilde{c} > 0.5\ (stage\ I) \end{cases} \tag{S11}$$

Concentration Boundary Conditions: The conservation of Li conservation admits the following boundary conditions: 1) $\hat{\boldsymbol{n}} \cdot (\kappa\nabla c)_s = \frac{\partial \gamma_s}{\partial c}$, where γ_s is the surface energy and $\hat{\boldsymbol{n}}$ is an outward facing unit normal vector. Although surface "wetting" has been shown to be important in nanoparticle dynamics [7], we set $\hat{\boldsymbol{n}}(\kappa\nabla c)_s = 0$ here. 2) The galvanostatic boundary condition $\frac{i}{e} = -\hat{\boldsymbol{n}} \cdot \boldsymbol{j}$.

Lithium plating: The electrochemical reaction associated with lithium plating is given by:

$$Li^+ + e^- \rightleftharpoons Li^0$$

The reaction can be described by symmetric (i.e. $\alpha = 0.5$) Butler-Volmer formulations. Herein we define two separate plating current densities: $i_{pl,m}$ based on the actual microscopic surface area of the edge plane being plated with Li (A_{Li}), varying with time as lithium nuclei grow/coalesce, and i_{pl} based on the projected area of the plated lithium nuclei onto the edge plane of the HOPG particle (A_p). Both current densities can be written as,

$$i_{pl,m} = i_{0,pl,m}\left[\exp(-\alpha\tilde{\eta}_{pl}) - \exp\left((1-\alpha)\tilde{\eta}_{pl}\right)\right] \tag{S12}$$

$$i_{pl} = i_{0,pl}\left[\exp(-\alpha\tilde{\eta}_{pl}) - \exp\left((1-\alpha)\tilde{\eta}_{pl}\right)\right] \tag{S13}$$

where we neglect the surface energy contribution to the overpotential in the microscopic reaction model [8] for simplicity, since the geometry is also changing rapidly and not known to have a certain shape, such as a hemisphere. Since both these expressions describe the same physical phenomena and must conserve charge, they are related as,

$$A_{Li} i_{pl,m} = A_p i_{pl} \implies A_{Li} i_{0,pl,m} = A_p i_{0,pl} \tag{S14}$$

The rate of lithium growth depends on the exposed microscopic surface area (A_{Li}) of deposited mossy lithium. As lithium nuclei grow, the ratio of the microscopic surface area to the projected area increases with time. By the law of conservation of charge, we equate the sum of the intercalation and plating currents to the applied current i as,

$$i A_{edge} = i_{int} A_{edge} + i_{pl} A_p \tag{S15}$$

The projected area of plated Li nuclei at the time of onset is assumed to be 1% of the left edge plane area A_{edge} of the HOPG particle, i.e. $A_p = 0.01 \times A_{edge}$. From the experimental videos, it can be visually estimated that the first observable lithium nuclei cluster growth occupies about 10% of the left edge length of the particle. Extending the same scaling to the depth dimension of the left edge plane as well, we estimate that the actual projected area of Li growth at onset is 1% of the left edge plane area of 0.1 mm^2.

The plating current contributes to the growth of deposited/plated lithium volume V_{Li} as:

$$\frac{1}{\Omega}\frac{dV_{Li}}{dt} = A_{Li}\frac{i_{pl,m}}{e} = A_p \frac{i_{pl}}{e} \tag{S16}$$

Here, we define $A_{Li} = A_{nuc}\left(\frac{V_{Li}}{V_{nuc}}\right)^{\beta}$. The choice $\beta = 2/3$ would describe normal non-fractal growth ($A \sim L^2$ and $V \sim L^3$ so $A \sim V^{2/3}$), including the prototypical case of a hemispherical nucleus. Over time, the exponent may decrease as nuclei merge into a film of nearly constant area ($\beta = 0$), or increase after highly ramified fractal dendrites form ($2/3 < \beta < 1$). Ω is the molar volume of lithium [9], and A_{nuc} and V_{nuc} are the total microscopic surface area and volume of the deposited lithium nuclei, which scales with the total number of nuclei N as, $A_{nuc} = A_{0,nuc} \times N$ and $V_{nuc} = V_{0,nuc} \times N$. $A_{0,nuc}$ and $V_{0,nuc}$ are the microscopic surface area and volume of a single lithium nucleus of critical radius that will spontaneously grow under the influence of current. The thermodynamic stability of a nucleus that deposits on an electrically charged substrate is determined by the bulk free energy of transformation, both chemical and electrical, and the surface tension contributions. For a single, isolated, hemispherical electrodeposit, the kinetic critical radius corresponding to the case where

the Laplace pressure balances the applied overpotential, is given by [9],

$$r^*_{nuc} = \frac{2\gamma\Omega}{zF\eta_{pl}} \tag{S17}$$

For an observed plating onset overpotential $\eta_{pl} \sim 0.15$ V vs. Li/Li^+ in our experiments (see Fig 5 in the main text), the kinetic critical radius r^*_{nuc} is approximately 0.75 nm. $A_{0,nuc}$ and $V_{0,nuc}$ for a growing hemisphere at critical radius subsequently can be calculated using $A_{0,nuc} = 2\pi {r^*_{nuc}}^2$ and $V_{0,nuc} = (2/3)\pi {r^*_{nuc}}^3$.

During growth of the mossy Li deposits, lithium nuclei merge into larger ones, leading to a transient variation of the total number of nuclei present in the system. However, since we are focused on the time regime of onset of plating, it is reasonable to assume that the number of nuclei N remains roughly constant in this period. The resolution of the experimental data is also insufficient to reliably extract information about nucleation and growth statistics, so we choose to forego the inclusion of a time dependent N whose distribution could be described using a Johnson-Mehl-Avrami-Kolmogorov (JMAK) modeling framework [10–12], in favor of a simpler model. We start with a monolayer coverage of lithium nuclei at kinetic critical radius covering the plating area A_p. So the total number of nuclei $N = A_p/A_{0,nuc} \sim 5.7 \times 10^8$. We note that N is a very large number, and the initial nuclei are far too small to be experimentally observed with an optical microscope. The resulting model should serve our purposes of accurately describing the onset of lithium plating on graphite, although not the long-time growth of significant mossy or dendritic deposits.

Additionally, by Equation S15 we assume that $i_{pl} \sim constant$ since $i_{int} \to 0$ after plating onset (see Figure 6D inset in main text). To obtain a time dependence of the plating exchange current and to verify the validity of the $i_{pl} \sim constant$ assumption, we perform a scaling analysis on Equation S16 which reveals a scaling of V_{Li} with time t as,

$$V_{Li} \approx \frac{A_p i_{pl} \Omega}{e}\, t \tag{S18}$$

Substituting this scaling into the relation for $i_{0,pl,m}$ and $i_{0,pl}$ in Equation S14, we get,

$$i_{0,pl,m} = i_{0,pl} \frac{A_p}{A_{nuc}} \left(\frac{eV_{nuc}}{A_p i_{pl} \Omega t_0} \right)^{\beta} \tilde{t}^{-\beta} \tag{S19}$$

The first two groups of variables in Equation S19 are known constants. t is non-dimensionalized by t_0, the time at which lithium nuclei surpass the critical radius r^*_{nuc}, at 3120s from the start of the experiment. Direct nanoscale observations of hemispherical lithium growth on a gold electrode by Kushima et al. [13] revealed that the size of the hemisphere grew roughly as the square root

of time (i.e. $R \sim t^{1/2}$) , which was quantitatively attributed to SEI growth on the deposited lithium. If the same mechanism were at work here, a microscopic exchange current density in 3D of $i_{0,pl,m} \propto t^{-1/2}$ would imply $\beta = 1/2$. Substituting back into Equation S16 with $\beta = 2/3$ for the hemispherical geometry, however, would yield a scaling $i_{pl} \propto t^{-1/2}t^{2/3} = t^{1/6}$, which is slowly varying and seemingly consistent with the original assumption that $i_{pl} \sim$ constant.

On the other hand, there are good reasons to expect additional mechanisms to slow down the microscopic plating reaction, which make the approximation of constant projected exchange current very reasonable, at least for the early stages of nucleation and growth of lithium metal. (1) The geometrical exponent β controlling the surface to volume ratio must slowly decrease from 2/3 (for separate hemispherical nuclei) as nuclei merge and coalesce and could decrease of even surpass $\beta = 1/2$ (for constant growth per projected area) since $\beta = 0$ is the value for dense flat film. (2) The number of nuclei will also decrease, as they merge to form a continuous deposit, and $N \sim t^{-1/2}$ could also justify the same result, with $\beta = 2/3$. (3) The microscopic overpotential has an additional contribution for curvature, which scales with inverse radius and decays with time as the initial nanoscale nuclei grow and merge into a film covering the surface. For all of these reasons, the detailed microscopic growth is quite complicated and yet consistent with the simple assumption of nearly constant macroscopic exchange current density $i_{0,pl}$ per projected area of lithium growth.

As plotted in Figure 5f in the main text, the voltage of the cell reaches a minimum value subsequent to which mossy lithium starts to deposit on the edge of the graphite particle. We propose that the offset of the voltage curve minimum from the 0 V line is the barrier for the first lithium nucleus to surpass the kinetic critical radius. The voltage barrier could have several physical origins - it could be influenced by the surface tension γ of lithium/electrolyte as the nucleus reaches the critical volume (see section: *Derivation of plating exchange current and degree of certainty*). It could also be the energy required for nucleation in the presence of a solid-electrolyte interphase (SEI) layer on the graphite active surface, in which case the critical voltage and critical radius might be a function of the cycling history of the cell. SEI also grows rapidly on fresh lithium nuclei [13] and thus the overpotential required for continued growth may deviate from that predicted by the classical nucleation theory framework presented in this paper.

Subsequent to spontaneous lithium nuclei growth on the edge-plane of graphite, the energy barrier for lithium growth becomes significantly smaller as the lithium wets the LiC_6 surface and the lack of vacant sites at graphite surface makes Li intercalation kinetically difficult. We define a barrier potential V_n, dependent on the volume of lithium deposited (V_{Li}) based on a Gaussian

function as,

$$V_n = V_{0,n} e^{-V_{Li}^2/2V_{nuc}^2} \tag{S20}$$

$V_{0,n}$ is assumed to be approximately 0.15 V from the experimental observations in Figure 5 in the main text. The exponential term ensures that the barrier potential goes to zero as the lithium content increases on the surface. The nucleation barrier affects the overpotential of the lithium plating reaction by lowering the equilibrium potential from 0 V as, $\eta_{pl} = \Delta\phi - (0 - V_n)$.

Numerical Methods: The domain is discretized in 1D with the left boundary as the graphite/electrolyte interface and the right boundary as a point inside the bulk of the HOPG particle where the bottom edge of the image slice is. The size of the slice is chosen such that the domain never becomes 'full' with lithium. This ensures that the simulation is always able to capture the interplay of bulk diffusion and surface intercalation at all time points in the experiment. The potential field $\phi(t)$ is assumed uniform in space as graphite is a good conductor of electrons, and only solved for in the time domain. The intercalated lithium concentration $c(x,t)$ is solved for evolution in space and time. The fourth-order Cahn-Hilliard equation (Eq. 2 in main text), the plated lithium growth equation S16, the barrier potential equation S20 and the constant current constraint equation S15 in the Equations section are solved as a system of differential algebraic equations (DAE). We take the general approach of discretizing each in space using some variant of the finite volume method to obtain the system of DAEs, and then stepping in time using a variable-order adaptive time stepper, ODE15s in MATLAB. We discretize in space using finite volume methods both for their robustness to steep gradients and also their mass conservation to within numerical accuracy. The width of a finite volume is chosen such that it is smaller than the interfacial width $\left(\lambda_b \sim \sqrt{\frac{\kappa}{c_{ref}\Omega_b}}\right)$ following Refs. [14] and [15]. The values of κ, c_{ref} and Ω_b of graphite are taken from Ref. [14]. The ODE15s function, based on a variant of the backward differentiation formula, handles the formation of all underlying system matrices and interactions with other numerical libraries involved in the time integration.

Some Additional Results: Our simulations demonstrate the predictability of the phase field model for graphite as it can qualitatively capture the observed Li ion concentration evolution in the particle. Additionally, Fig. 6D in the main text demonstrates the fitted and experimentally observed voltage vs. charge profiles. Fig. 6E in the main text depicts the the model predictions on the voltage V and surface concentration c_s under delithiation.

The model can predict the onset of Li plating and the correct value of the nucleation voltage. As discussed in Fig. 5 based on the experimental observations, Li plating occurs only when the surface of graphite becomes saturated by the inserted Li ions. Fig. S11 demonstrates the evolution of the surface concentration as a function of the average Li fraction in the graphite particle. Our calculations show that when the surface concentration c_s becomes 1 the nucleation barrier is exceeded. Furthermore, a solid solution model (Figure S11 e-h) is insufficient in its ability to predict the onset of lithium plating correctly. Fig. S12 depicts the predicted rest and delithiation profiles, corresponding to the potential curves shown in Fig 6E in the main text. Upon comparison with experimental results in Figure 4 in the main text, one can conclude that the model, fitted only to lithiation voltage profiles, can predict the system behavior during rest and delithiation reasonably well. During rest, some of the plated Li dissolves, contributing to further intercalation into the active material. This can be thought of as self-discharge of a local short-circuited battery comprising the plated Li and graphite surface. Delithiation shows simultaneous dissolution of the plated Li as well as slow de-intercalation from the active particle. Initially, most of the stripping occurs at the plated lithium, and the graphite surface in equilibrium with the plated Li stays at $c_s \sim 1$. Once all plated Li has been completely depleted from the system, the surface concentration immediately drops and a traversing delithiation front in the active material is observed, as expected.

Derivation of plating exchange current and degree of certainty: In our simulation, we find the plating exchange current based on projected area $i_{0,pl}$ to be 2.2 A/m^2 and the one based on microscopic surface area $i_{0,pl,m}$ to be 7×10^3 $\tilde{t}^{-1/2}$ A/m^2, where we report only one significant digit, due to uncertainty in active area and other parameters. Despite the seemingly crude approximations here, however, we believe this value is the most accurate to date, since we directly observe the active region of metal growth, while fitting to a model that captures the coupling to intercalation with validation from other experiments.

A browse through literature to compare our obtained exchange current value reveals there is little agreement on its order of magnitude: values of $i_{0,pl}$ ranging from 10^{-3} A/m^2 to 10^2 A/m^2

have been reported for lithium growth on carbon electrodes [13, 16–19]. To our knowledge, this is the first estimation of plating exchange current from direct in-situ optical data. The order of magnitude of the initial value of exchange current $i_{0,pl} \sim 2.2\ A/m^2$ agrees well with that reported by the direct measurements of Kushima et al. [13]. However, since visual estimation of growing lithium nuclei is challenging, since individual Li whiskers can be on the order of a few hundred nanometers [13], our theoretical prediction is primarily an order-of-magnitude estimate resulting from the growth of the first cluster of plated lithium nuclei.

The lithium-organic electrolyte interfacial energy γ is an important thermodynamic parameter describing the kinetic critical radius of lithium nuclei during the onset of plating. It also affects the degree of certainty in the prediction of the plating exchange current $i_{0,pl}$. In this work, we use reported by Lu et al. [20] which was derived out of direct experimental measurements of contact angles of various organic electrolytes on pure Li metal in an inert atmosphere at steady state. In their work, analysis of the contact angle data to determine surface tension γ was done using Young's equation and the Zisman approach [21–23]. Historically, due to absence of direct experimental measurements, theoretical results from Mullins-Sekerka type linear stability analyses were used to describe electrodeposition of metals in aqueous electrolytes [8, 24–26]. Aogaki and Makino (1979) [25], and Sundstrom and Bark (1995) [26] independently established the theory for interfacial stability for metal electrodeposition in aqueous systems using linear stability analysis. In 1998, Yamaki et al. [27] used the above theories to recommend a lower bound to the value of interfacial energy for lithium-organic electrolyte systems, approximately $0.2Nm^{-1}$, in absence of any experimental data at the time. Interestingly, these results have been widely used in lithium nucleation and growth modeling in organic electrolytes without any validation until as recently as 2017 [9, 28–30]. Upon comparison to the direct experimental results of Lu et al. [20], one can find that the interfacial energy recommendation by Yamaki et al. and predecessors and consequently that of contemporary lithium nucleation models are erroneous by about one order of magnitude. Admittedly, the contact angle measurements done by Lu et al. [20] are at steady-state and one could expect a deviation of the actual interfacial energy in unsteady state systems such as growing lithium nuclei on graphite. One way this could be directly validated is by observing in-situ critical nucleus size (using high resolution techniques such as in-situ atomic force microscopy or high-energy X-ray diffraction) and correlating the observed nucleation barrier V_n to the interfacial energy using Eq. S17. We will address this uncertainty and benchmark the theory against direct critical radius measurements using a porous electrode model in a future publication.

List of parameters:

Variable	Description	Value	Reference
$k_{0,int}$	Intercalation exchange current	1 A/m^2	[14]
$i_{0,pl}$	Plating reaction rate constant based on projected surface area	2 A/m^2	fitted
$i_{0,pl,m}$	Plating reaction rate constant based on microscopic surface area	7×10^3 $\tilde{t}^{-1/2}$ A/m^2	fitted, Eq. S19
N	Number of growing Li nuclei during plating	5.7×10^8	assumed
$V_{0,n}$	Nucleation potential for critical volume	0.15 V	experiments
A_{edge}	Edge-plane area for HOPG particle	0.1 mm^2	experiments
λ	Reorganization energy for graphite intercalation	$5k_BT$	[31, 32]
Ω	Molar volume of lithium	12.99 cm^3/mol	[9]
γ	Li-electrolyte interfacial energy	0.49 J/m^2	[20]

The equation for the homogeneous chemical potential μ_h is taken from Appendix A of Ref [4],

given below:

$$\mu_h = 0.18 + \mu_a + \mu_b + \mu_c + \mu_d + \mu_e$$

$$\mu_a = RT\left[\left(-40exp\left(-\frac{\tilde{c}}{0.015}\right) + 0.075\left(\tanh\left(\frac{\tilde{c}-0.17}{0.02}\right) - 1\right) + \tanh\left(\frac{\tilde{c}-0.22}{0.04} - 1\right)\right) S_D(\tilde{c}, 0.35, 0.05)\right]$$

$$\mu_b = -RT\frac{0.05}{\tilde{c}^{0.85}}$$

$$\mu_c = 10RTS_U(\tilde{c}, 1, 0.045)$$

$$\mu_d = 6.12RT(0.4 - \tilde{c}^{0.98})S_D(\tilde{c}, 0.49, 0.045)S_U(\tilde{c}, 0.35, 0.05)$$

$$\mu_e = RT(1.36(0.74 - \tilde{c}) + 1.26)S_U(\tilde{c}, 0.5, 0.02)$$

$$S_U(x, x_c, \delta) = 0.5\left(\tanh\left(\frac{x - x_c}{\delta}\right) + 1\right)$$

$$S_D(x, x_c, \delta) = 0.5\left(-\tanh\left(\frac{x - x_c}{\delta}\right) + 1\right)$$

* Corresponding author: bazant@mit.edu

[1] M. Z. Bazant, Accounts of Chemical Research **46**, 1144 (2013), arXiv:arXiv:1208.1587v5.

[2] A. Pei, G. Zheng, F. Shi, Y. Li, and Y. Cui, Nano letters **17**, 1132 (2017).

[3] G. Wertheim, P. T. M. Van Attekum, and S. Basu, Solid State Communications **33**, 1127 (1980).

[4] K. E. Thomas-Alyea, C. Jung, R. B. Smith, and M. Z. Bazant, Journal of The Electrochemical Society **164**, E3063 (2017).

[5] J. W. Cahn and J. E. Hilliard, Journal of Chemical Physics **28**, 258 (1958).

[6] K. Persson, Y. Hinuma, Y. S. Meng, A. Van der Ven, and G. Ceder, Physical Review B **82**, 125416 (2010).

[7] D. A. Cogswell and M. Z. Bazant, Nano Letters **13**, 3036 (2013), 1304.0105.

[8] E. Khoo, H. Zhao, and M. Z. Bazant, Journal of The Electrochemical Society **166**, A2280 (2019).

[9] D. R. Ely and R. E. García, Journal of the Electrochemical Society **160**, A662 (2013).

[10] A. N. Kolmogorov, *On the Statistical Theory of Crystallization of Metals [in Russian]* (Izv. Akad. Nauk SSSR, Ser. Mat. No. 3, 1937).

[11] M. Avrami, J. Chem. Phys **8**, 212 (1940).

[12] J. William and R. Mehl, Trans. Metall. Soc. AIME **135**, 416 (1939).

[13] A. Kushima, K. P. So, C. Su, P. Bai, N. Kuriyama, T. Maebashi, Y. Fujiwara, M. Z. Bazant, and J. Li, Nano Energy **32**, 271 (2017).

[14] R. B. Smith, E. Khoo, and M. Z. Bazant, The Journal of Physical Chemistry C **121**, 12505 (2017).

[15] Y. Zeng and M. Z. Bazant, SIAM Journal on Applied Mathematics **74**, 980 (2014).

[16] H. Ge, T. Aoki, N. Ikeda, S. Suga, T. Isobe, Z. Li, Y. Tabuchi, and J. Zhang, Journal of The Electrochemical Society **164**, A1050 (2017).

[17] P. Arora, M. Doyle, and R. E. White, Journal of The Electrochemical Society **146**, 3543 (1999).

[18] X.-G. Yang, Y. Leng, G. Zhang, S. Ge, and C.-Y. Wang, Journal of Power Sources **360**, 28 (2017).

[19] C. von Lüders, J. Keil, M. Webersberger, and A. Jossen, Journal of Power Sources **414**, 41 (2019).

[20] Y. Lu, Z. Tu, and L. A. Archer, Nature materials **13**, 961 (2014).

[21] W. A. Zisman, Industrial & Engineering Chemistry **55**, 18 (1963).

[22] M. Gindl, G. Sinn, W. Gindl, A. Reiterer, and S. Tschegg, Colloids and Surfaces A: Physicochemical and Engineering Aspects **181**, 279 (2001).

[23] M. Dahbi, D. Violleau, F. Ghamouss, J. Jacquemin, F. Tran-Van, D. Lemordant, and M. Anouti, Industrial & engineering chemistry research **51**, 5240 (2012).

[24] C. P. Nielsen and H. Bruus, Physical Review E **92**, 052310 (2015).

[25] R. Aogaki and T. Makino, Electrochimica Acta **26**, 1509 (1981).

[26] L.-G. Sundström and F. H. Bark, Electrochimica acta **40**, 599 (1995).

[27] J.-i. Yamaki, S.-i. Tobishima, K. Hayashi, K. Saito, Y. Nemoto, and M. Arakawa, Journal of Power Sources **74**, 219 (1998).

[28] R. Akolkar, Journal of Power Sources **232**, 23 (2013).

[29] D. Wang, W. Zhang, W. Zheng, X. Cui, T. Rojo, and Q. Zhang, Advanced Science **4**, 1600168 (2017).

[30] C. Monroe and J. Newman, Journal of The Electrochemical Society **150**, A1377 (2003).

[31] D. Fraggedakis, M. McEldrew, R. B. Smith, Y. Krishnan, Y. Zhang, W. Chueh, P. Bai, Y. Shao-Horn, and M. Z. Bazant, "Theory of coupled ion-electron transfer kinetics," (2020).

[32] D. Fraggedakis, Y. Zhang, T. Gao, R. M. Stephens, Y. Shao-Horn, and M. Z. Bazant, (2020).

SUPPLEMENTARY FIGURES

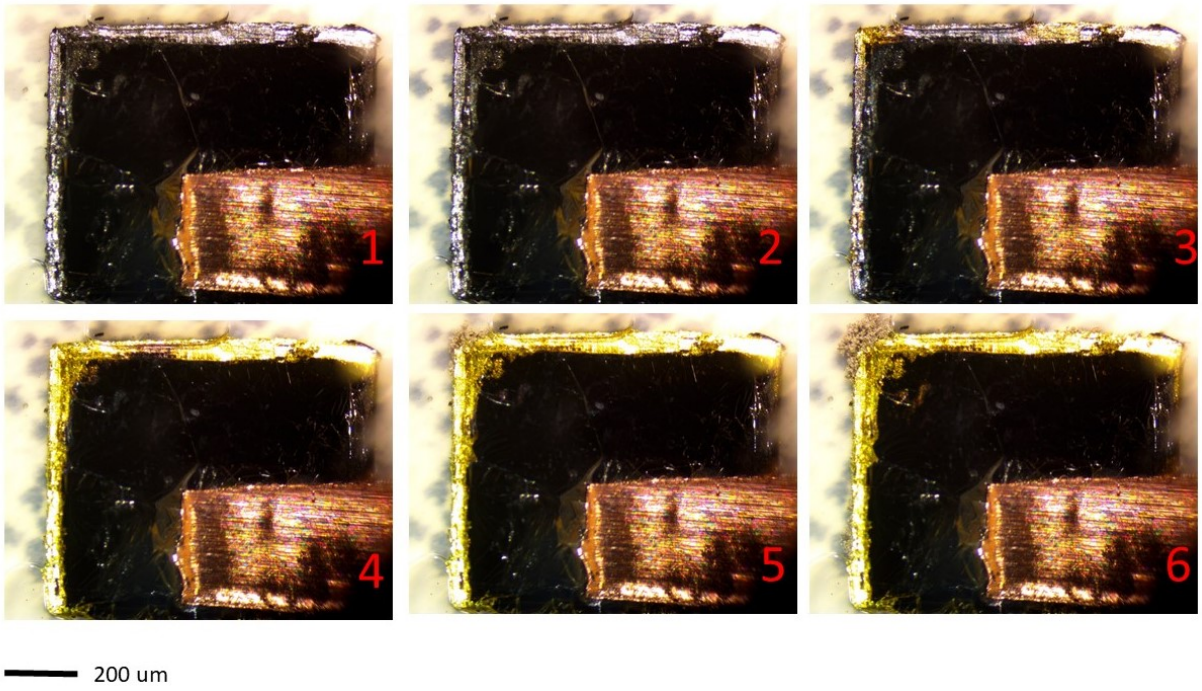

FIG. S1. The lithiation of HOPG particle A

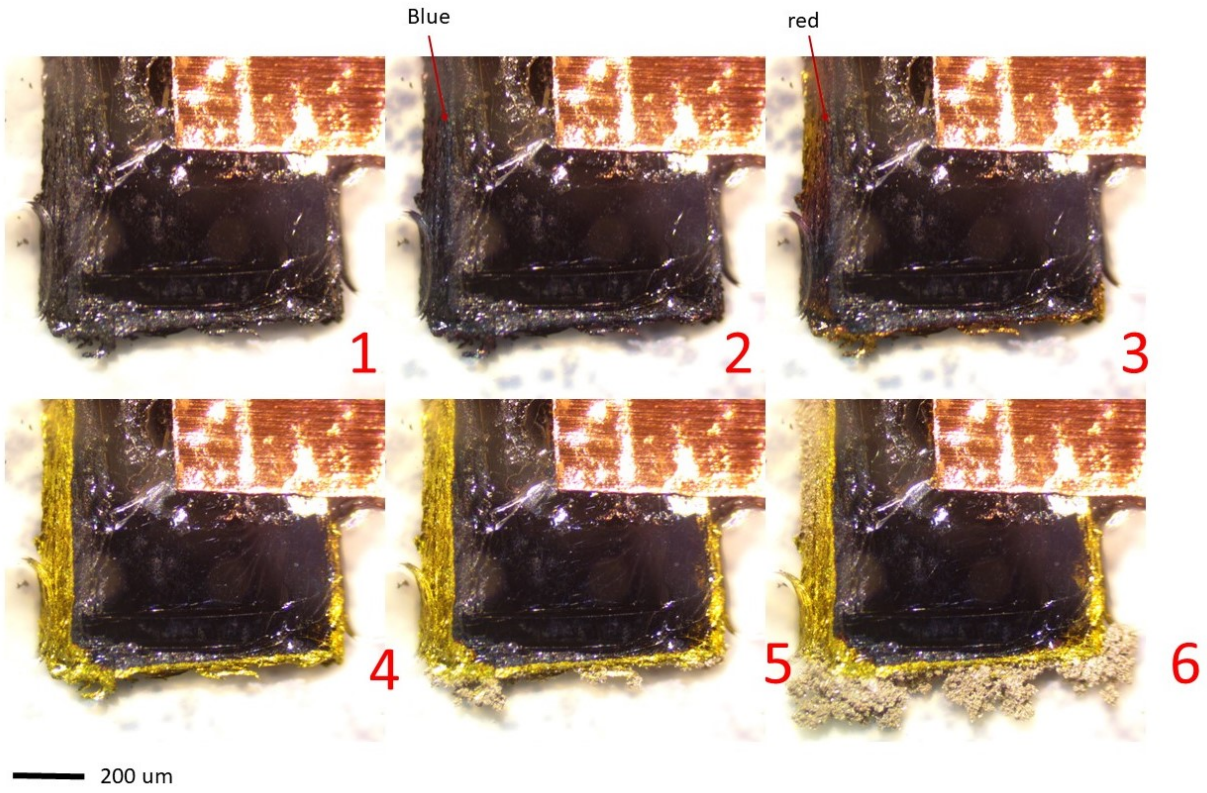

FIG. S2. The lithiation of HOPG particle C

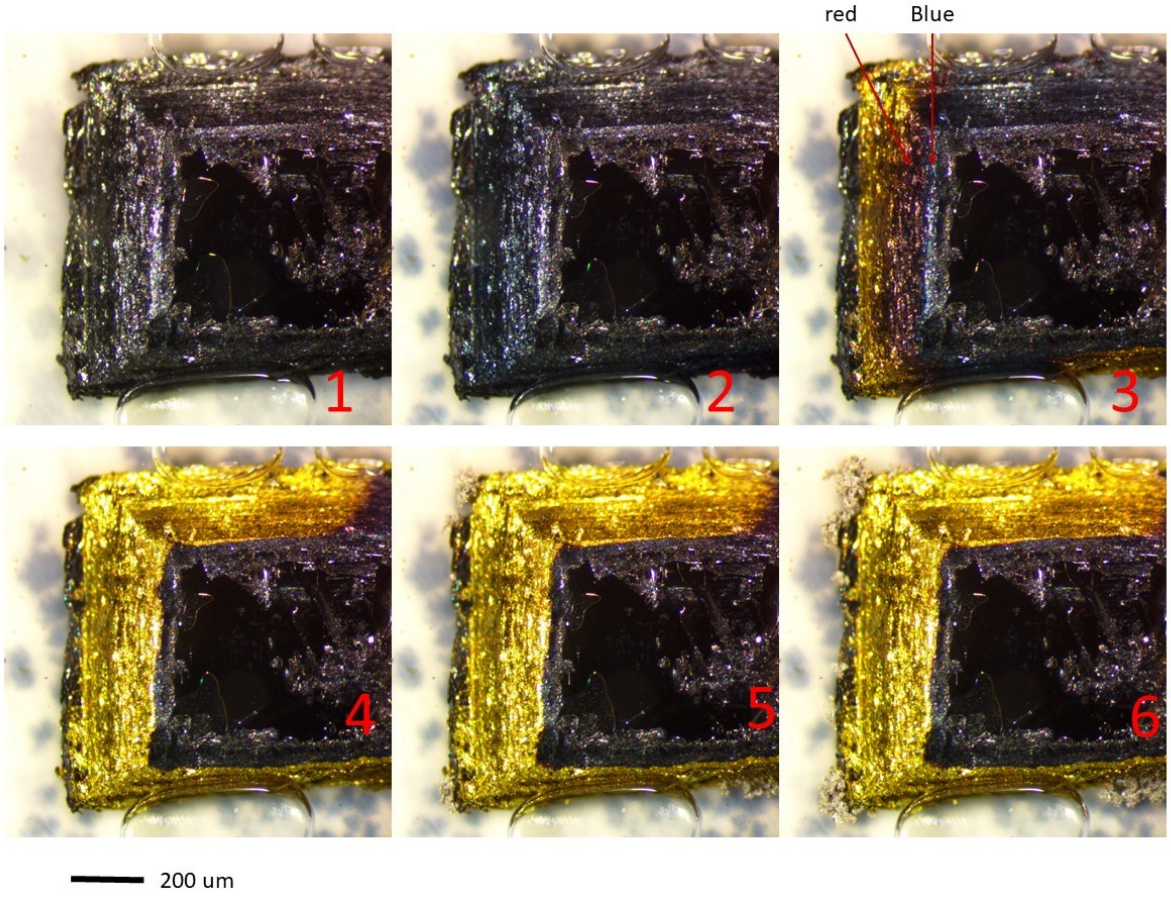

FIG. S3. The lithiation of HOPG particle D

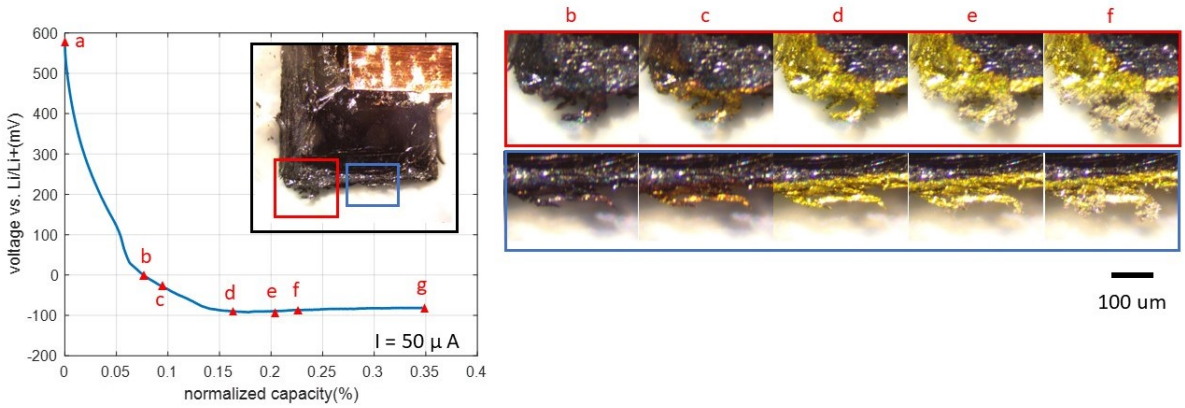

FIG. S4. voltage and zoom-in images of particle C

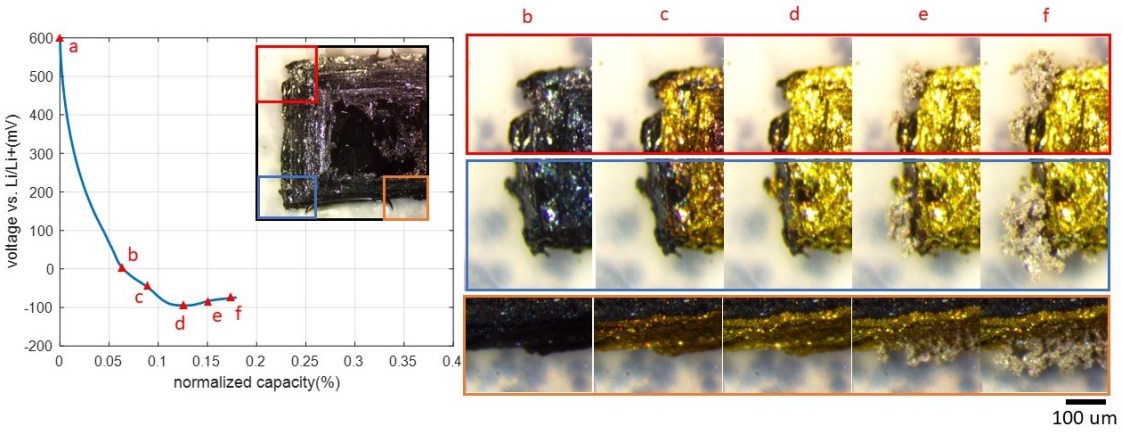

FIG. S5. voltage and zoom-in images of particle D

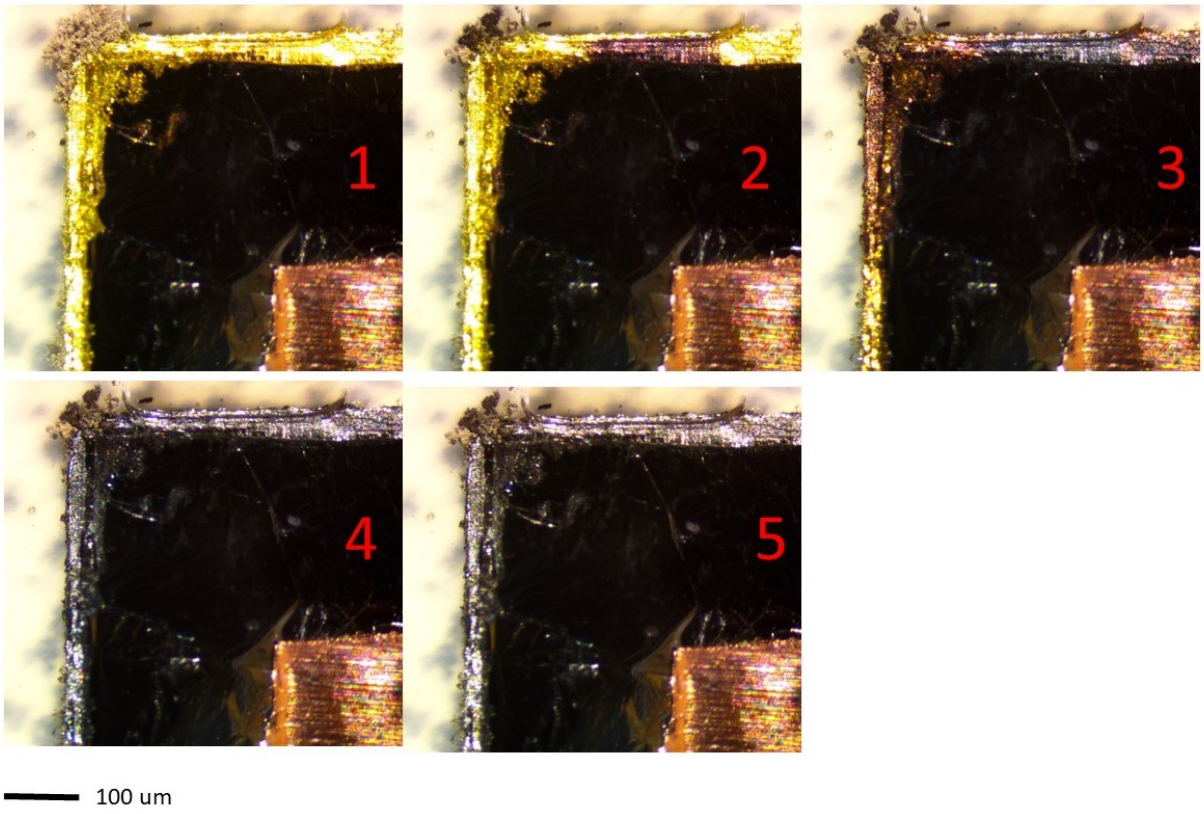

FIG. S6. The rest of HOPG particle A

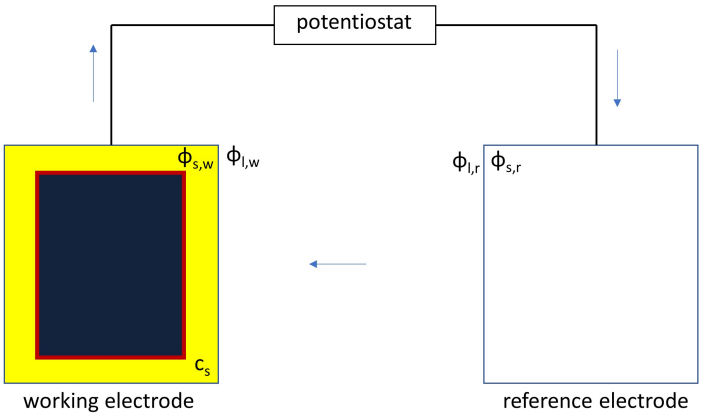

FIG. S7. **schematic for reactions at working and reference electrode**

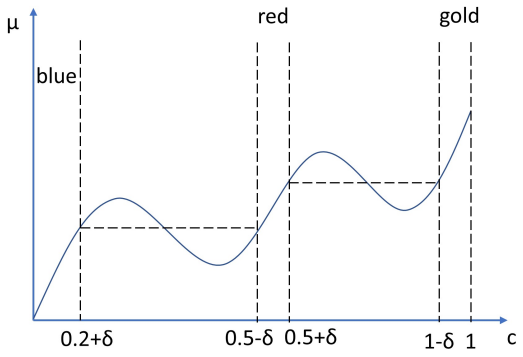

FIG. S8. **Diffusional chemical potential as a function of local concentration**

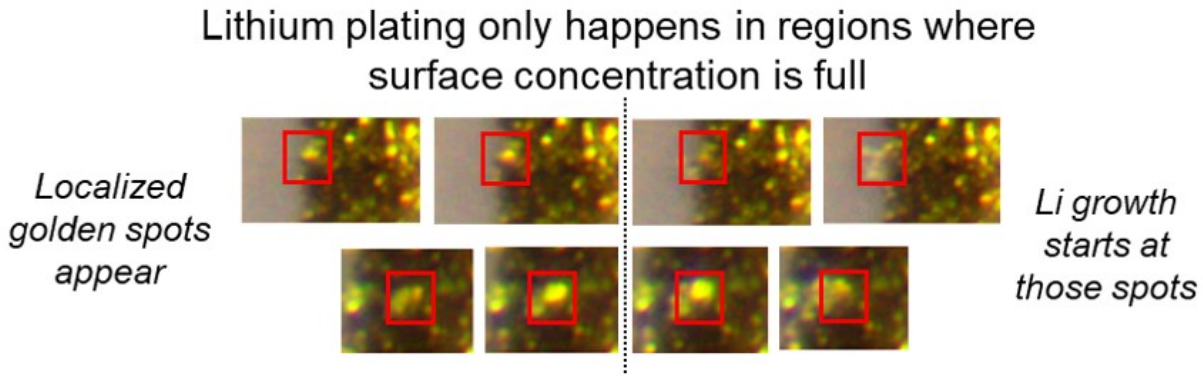

FIG. S9. **Snapshots of points on electrode, that turn from bright gold to silver, demonstrating that mossy lithium nucleates and grows only from regions where particles are full**

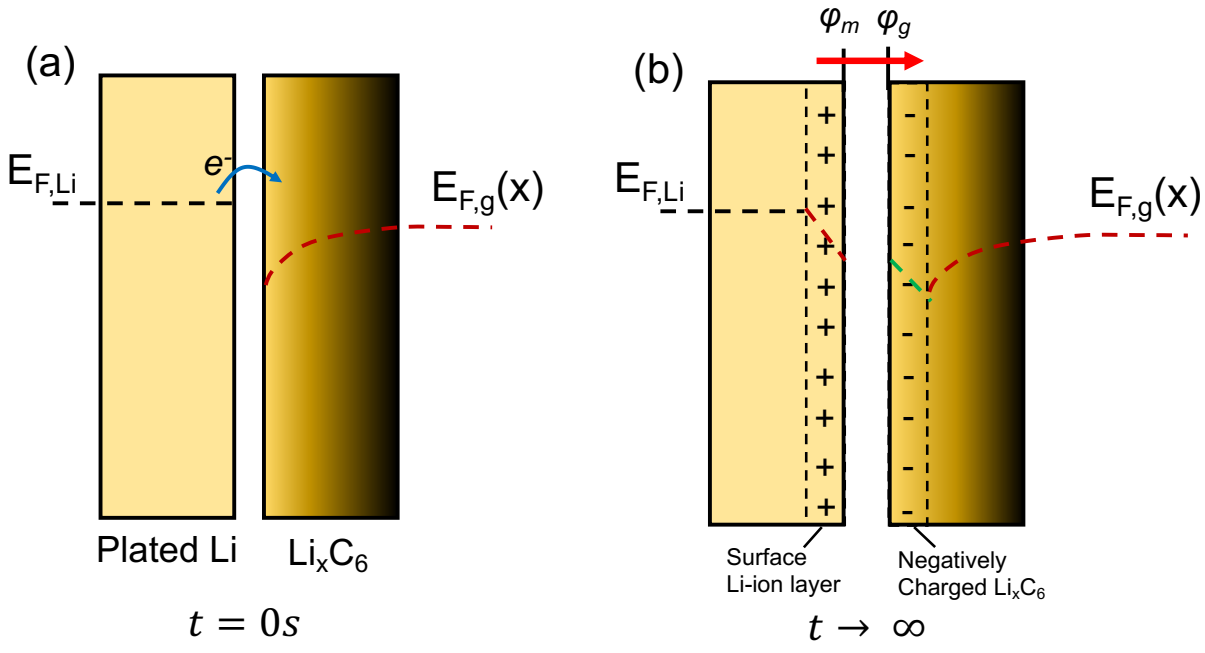

FIG. S10. **schematic for the formation of contact potentials**

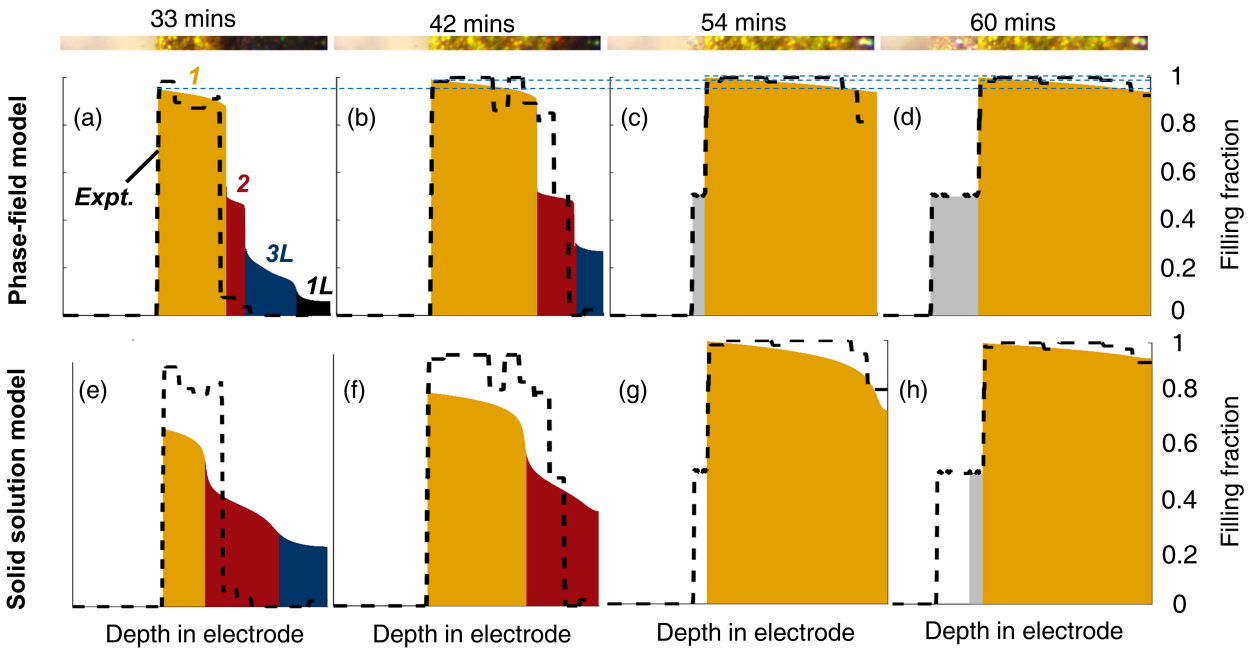

FIG. S11. Model predictions of Li concentration profiles compared with experimental data during lithiation, under a driving current I = 5 mA/cm^2. (a-d) Cahn-Hilliard Reaction model (e-h) Solid solution model

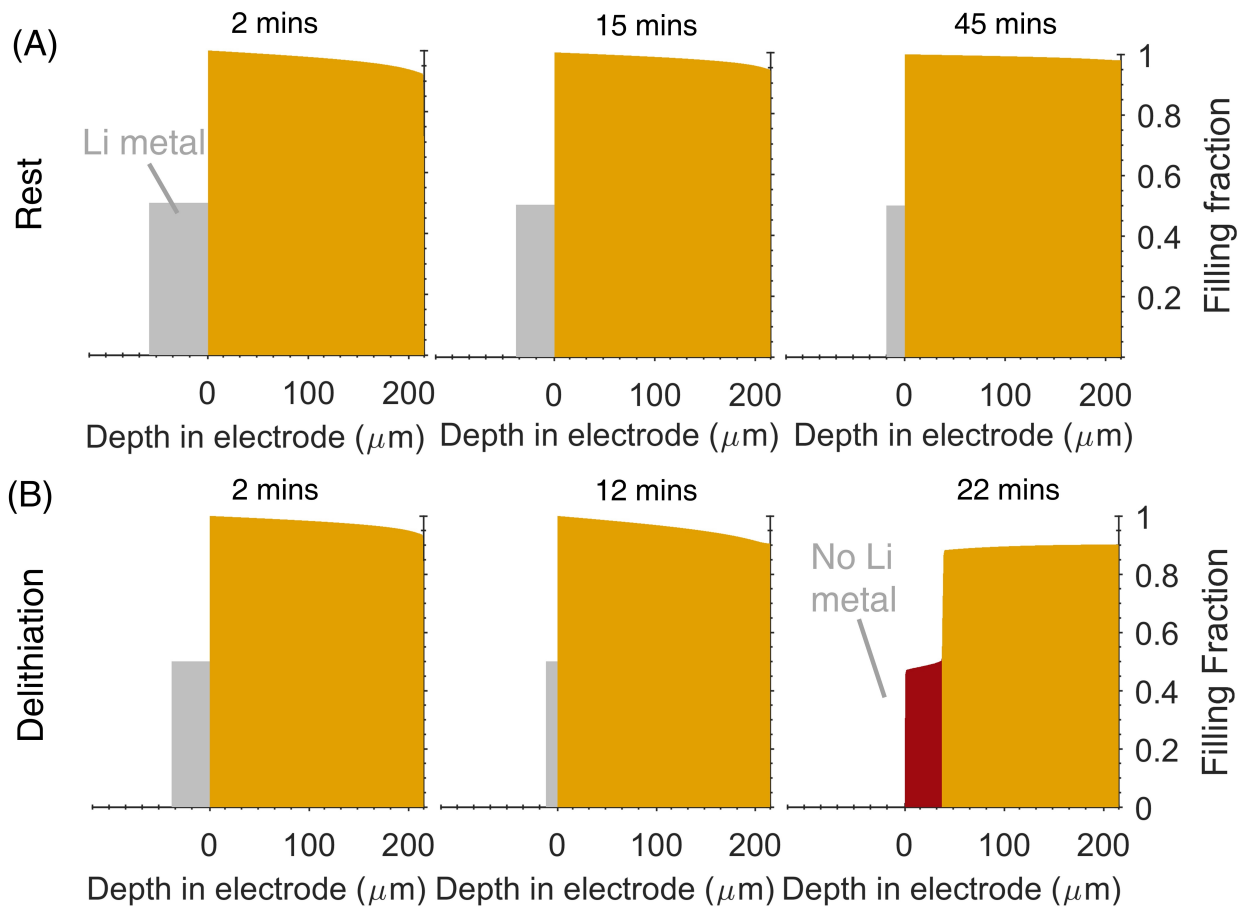

FIG. S12. Model predictions of Li concentration profiles (A) during 45 min rest and (B) under delithiation with a driving current I = 5 mA/cm^2